Synthesis, Structure, and Reactivity of a New Ti-Containing Microporous/Mesoporous Material

Sean M. Solberg, Dharmesh Kumar, and Christopher C. Landry*

Department of Chemistry, University of Vermont, 82 University Place, Burlington, Vermont 05405

Received: July 28, 2005; In Final Form: October 27, 2005

A new class of porous, mixed phase titanosilicate materials containing a microporous TS-1 phase and a mesoporous Ti-MCM-48 phase has been successfully synthesized. A novel, one-pot synthesis method was used in which the organic templates for the mesoporous and microporous phases were added sequentially to the same reaction mixture, followed by crystallization at 150 °C. The gemini surfactant 18-12-18 was used to form the Ti-MCM-48 mesophase; subsequent addition of tetrapropylammonium cation (TPA^+) led to the formation of TS-1. The relative amounts of the two phases within the final products were controlled by optimizing the crystallization time. Crystallization times between 12 and 50 h gave materials containing both phases, with an increasing amount of microphase formed at longer crystallization times. These materials, called "Ti-MMM-2" (*m*icroporous/*m*esoporous *m*aterials) were characterized using powder XRD, N_2 physisorption, TEM, FTIR, DR-UV/Vis spectroscopy, and ^{29}Si MAS NMR. In the epoxidation of cyclohexene with *tert*-butyl hydroperoxide (TBHP), Ti-MMM-2 samples exhibited higher catalytic activity (∼61%) than either TS-1 (16%) or Ti-MCM-48 (42%), with a very high selectivity (97%) for formation of cyclohexene oxide.

Introduction

Ordered mesoporous silica materials have recently been the subject of intense research in the fields of catalysis and materials science.[1,2] The narrow and controllable pore size distributions, relatively large pore openings, large surface areas, greater adsorption capacities, and various other properties of these materials have led to their application in catalysis.[3] Mesoporous materials have often been doped with heteroatoms,[3−5] with the intention of developing materials that exhibit the requisite activity and selectivity for specific catalytic reactions. In particular, Ti-doped mesoporous molecular sieves such as Ti-MCM-41 and Ti-MCM-48 have been used to study the epoxidation of unsaturated alcohols, hydrocarbons, and a number of other organic compounds.[6−10] Ti-MCM-48 was found to exhibit better activity than Ti-MCM-41, presumably due to its highly interconnected, three-dimensional pore structure, which allowed the organic substrates better access to the reaction surface of the substrate.[8] Several researchers have attempted to improve the hydrophobicity of Ti-MCM-41 and Ti-MCM-48 by postsynthetic silylation of their surfaces, a process which was found to remarkably enhance their catalytic activities.[11,12] The persistent limitation of mesoporous materials arises from thermal instability due to the amorphous nature of the pore walls. On the other hand, zeolites and related crystalline microporous materials are widely used in industry as catalysts due to their excellent thermal stability. For example, titanium silicates such as TS-1, Ti-β, and Ti-MWW show excellent potential as oxidation catalysts of various organic substrates.[13,14] However, these microporous materials have pore diameters smaller than 7 Å and cannot catalyze the oxidation of bulky organic molecules due to the inaccessibility of active sites located inside the micropores. This strongly limits the application of Ti-substituted zeolites for the catalytic oxidation of these types of organic substrates.

A significant effort has been focused on combining the advantages of large pore mesoporous materials with those of zeolites. Several synthetic approaches have been used to prepare materials containing both mesoporous and microporous phases. Kloetstra et al. succeeded in synthesizing an MCM-41 material with zeolitic walls through a two-step recrystallization process.[15] Similar methods have yielded other "mixed phase" materials.[16−18] In contrast, Pinnavaia et al. utilized preformed zeolite seeds as building blocks to synthesize stable mesoporous aluminosilicates.[19] Kaliaguine et al. prepared a mixed phase mesoporous material where the mesoporous aluminosilicate was coated with zeolite.[20] Almost all of these mixed-phase materials have contained the one-dimensional, hexagonally structured mesophase MCM-41. Only a few groups have reported composite materials with the MCM-48 mesophase, which would be expected to perform better during catalysis. The lack of publications in this area may reflect a difficulty in synthesizing the cubic phase material. Bein et al. recently reported a MCM-48/zeolite-β aluminosilicate material synthesized by a simultaneous hydrothermal treatment process.[21] An MCM-48/MFI aluminosilicate composite was also recently prepared by Mokaya et al. using a two-step crystallization procedure.[22] Finally, although much work has been performed on mixed phase aluminosilicate materials, only few reports exist on mixed phase titanium composites, and none of these materials contained a cubic mesostructure.[23−25]

Our research group recently prepared MCM-41/MFI mixed phase silicate and aluminosilicate materials, designated "MMM-1" for *m*icroporous/*m*esoporous *m*aterial, by direct addition of TPA^+ to the synthesis mixtures after the mesoporous phase had begun to form, followed by crystallization at temperatures above 150 °C.[26,27] The synthetic method used in those experiments took advantage of the fact that at short polymerization times

* To whom correspondence should be addressed. Fax: +1 802 656 0270. E-mail: christopher.landry@uvm.edu.

10.1021/jp054187y CCC: $30.25
Published on Web 12/01/2005

the growing mesophase (containing a "primary" organic surfactant template) had a low degree of polymerization and a relatively high surface charge and therefore could incorporate a secondary organic template for zeolite formation into the incompletely polymerized mesophase network walls. Subsequent heating to temperatures at which zeolite formation occurred led to the localized formation of zeolitic structures within the mesoporous material; however, without heating, zeolite formation did not occur and only the mesoporous structure was formed. Therefore, a single reaction mixture could be used to produce multiple materials simply by adjusting the crystallization temperature and time. This strategy represents a simple, one-pot method for producing composite systems. In addition, with slight adjustment of reaction conditions, heteroatoms could be incorporated into the mixed phase materials. We also reported on a Ti-doped mixed-phase catalyst, named Ti-MMM-1, that contained Ti-MCM-41 and TS-1 phases. Interestingly, this material exhibited several unique properties that distinguished it from pure Ti-MCM-41 and pure TS-1, such as higher catalytic activity for the oxidation of cyclohexane and octane.[26] Ti-MMM-1 also showed a higher selectivity for the monooxidized products of each compound. This indicated a unique Ti environment and an intimately connected porous framework rather than a physical mixture of microporous and mesoporous phases. In continuation of the previous work, this paper describes the synthesis of a mixed phase material containing a Ti-MCM-48 mesophase and a TS-1 microphase, which we have designated Ti-MMM-2. During the synthesis of this material, the growing three-dimensional cubic mesostructure has been manipulated to form microphase in situ.[28,29] The methodology described above has been extended to the Ti-containing cubic mesoporous system, and microporous character has been controlled by the addition of a secondary template and by manipulating the crystallization time.[26,27] The synthesized materials have been characterized using powder X-ray diffraction (XRD), N_2 physisorption, diffuse reflectance UV−visible spectroscopy, FTIR, ^{29}Si MAS NMR, and transmission electron microscopy (TEM). The catalytic activities and selectivities of Ti-MMM-2 for the epoxidation of cyclohexene are compared to those of pure Ti-MCM-48 and pure TS-1.

Experimental Section

Materials and Methods. Powder X-ray diffraction (XRD) experiments were performed on a Scintag X1 $\theta-\theta$ diffractometer equipped with a Peltier detector using Cu Kα radiation ($\lambda = 1.5456$ Å). Nitrogen adsorption and desorption isotherms were obtained at 77 K on a Micrometrics ASAP 2010 instrument. Samples were degassed at 200 °C under vacuum overnight prior to measurement. Surface area and pore size distributions were calculated from the BET and the BJH methods, respectively. A Perkin-Elmer system 2000 spectrophotometer was employed to record the FTIR spectra. Compressed KBr pellets containing about 2 wt % of a sample were used for IR studies. The solid-state ^{29}Si MAS NMR spectra were measured on a Bruker model ARX-500 spectrometer at a resonance frequency of 99.35 MHz. The powdered samples were placed in 7.0 mm diameter zirconia rotors and spun at a rate of 4.0 kHz. A 30 s recycle delay was used between pulses. The chemical shifts were referenced to 3-(trimethylsilyl)-1-propanesulfonic acid sodium salt. Diffuse reflectance UV−visible spectra were recorded on a Perkin-Elmer Lambda 35 spectrophotometer with a LabSphere integrating sphere. $BaSO_4$ was used as the reference material, and the Kubelka−Munk function was used to obtain the data. TEM images were recorded with a JEOL JEM 1210 instrument operating at 120 kV. Samples were ultrasonicated in ethanol and dispersed on carbon films supported on copper grids. Chemical analyses were performed by Robertson Analytical Services. The surfactant $[CH_3(CH_2)_{17}N^+(CH_3)_2(CH_2)_{12}N^+(CH_3)_2(CH_2)_{17}CH_3]Br_2$, abbreviated 18-12-18, was synthesized from a previously published procedure.[30] NaOH was purchased from J. T. Baker. All other chemicals were purchased from Aldrich and were used as received.

Synthesis of Ti-MMM-2. A Ti-containing solution was prepared by adding H_2O_2 (30 wt % in H_2O, 0.3 g, 2.65 mmol) and 1 mL of deionized water to $Ti(O^nBu)_4$ (0.0254 g, 0.149 mmol). This solution was stirred for 30 min. In a separate beaker, the gemini surfactant 18-12-18 (0.37 g, 0.40 mmol) was dissolved in a solution containing H_2O (16.33 g) and 2 M NaOH (2.38 g, 41 mmol), which was then heated at 60 °C to dissolve the surfactant. Upon cooling, Ludox colloidal silica (1.49 g, 30 wt % in water) was added and the mixture was stirred briefly. The titanium solution was then added slowly to the surfactant-containing solution, and stirring was continued for 180 min before the addition of tetrapropylammonium bromide (TPABr, 0.25 g, 0.94 mmol). Stirring was continued overnight, and then the gel was transferred to a Teflon-lined Parr autoclave and crystallized at 150 °C for various time intervals between 10 and 80 h. The product obtained was filtered, washed extensively with deionized water, and dried at 100 °C overnight. Calcination to remove the organic templates was performed by heating the composite material to 550 °C at a rate of 2 °C/min in air, followed by a 12 h hold at that temperature.

Synthesis of Ti-MCM-48. To keep the synthesis conditions as consistent as possible for all samples, Ti-MCM-48 was synthesized following the above procedure with the exception that the secondary template was omitted. The samples were crystallized at 150 °C for 20 h. The resulting white solid was collected by filtration and calcined according to the method described above. Ti-MCM-48 could also be prepared by adding the secondary template as above and omitting the heating step.

Synthesis of TS-1. $Ti(O^nBu)_4$ (0.172 g, 0.51 mmol), H_2O_2 (30 wt % in H_2O, 0.3 g, mmol), and 2 mL of H_2O were stirred in a beaker for 30 min. $Si(OEt)_4$ (10 g, 48 mmol), tetrapropylammonium hydroxide (1 M in H_2O, 15 g, 12 mmol), and 14 mL of H_2O were then added, and the resulting mixture was stirred for 3 h. The mixture was then transferred to a Teflon-lined Parr autoclave and heated at 170 °C for 48 h. The white solid was collected by filtration and calcined according to the method described above.

Catalytic Activity Studies. The epoxidation of cyclohexene was carried out in a round-bottom flask equipped with a condenser. Ti-containing catalyst (0.20 g, dried overnight at 110 °C), cyclohexene (0.082 g, 1 mmol), *tert*-butyl hydroperoxide (TBHP, 5.5 M in decane, 0.2 mL, 1.1 mmol), and CH_2Cl_2 (5 mL) were then added, and the mixture was stirred at 40 °C for 24 h. The reaction products were filtered and analyzed on an Agilent model 6890 gas chromatograph equipped with a flame ionization detector, using a 5% phenylmethylsiloxane capillary column. The products were further confirmed on a mass spectrometer connected to a gas chromatograph using a HP-5MS column (J&W Scientific, 15 m × 0.32 cm).

Results and Discussion

Gemini surfactants of the type $[C_nH_{2n+1}N^+(CH_3)_2(CH_2)_sN^+(CH_3)_2C_mH_{2m+1}]Br_2$, with the abbreviated name "n-s-m", have been shown to promote the formation of mesoporous materials under a range of synthesis conditions. The surfactant 18-12-18 was chosen because it easily forms the cubic MCM-48 phase

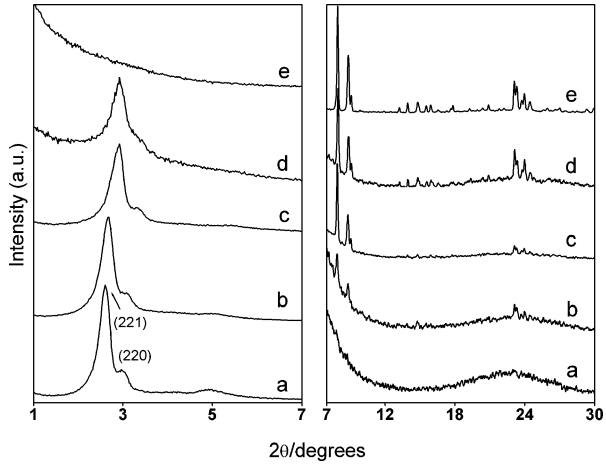

Figure 1. Powder XRD patterns of calcined Ti-MMM-2 in the mesophase (1−7°) and microphase (7−30°) regions of the patterns. Samples were crystallized at 150 °C for (a) 12 h, (b) 20 h, (c) 30 h, (d) 50 h, and (e) 80 h. Note the different vertical and horizontal scales of the two regions.

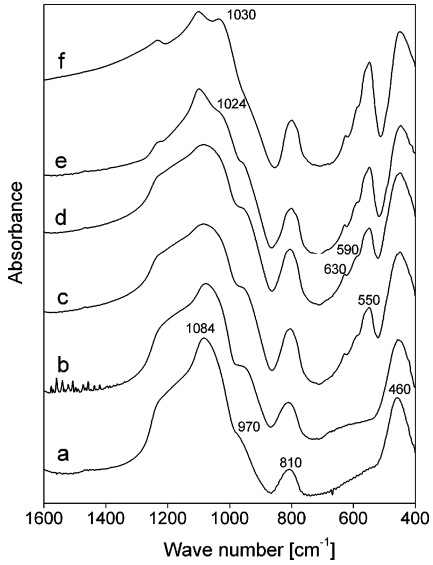

Figure 2. IR spectra of (a) calcined Ti-MCM-48 and calcined Ti-MMM-2 samples crystallized at 150 °C for (b) 12 h, (c) 20 h, (d) 50 h, and (e) 80 h. The spectrum of TS-1 is shown in part f.

under standard conditions.[30,31] Using this surfactant as the primary organic template, and adding TPA^+ as the secondary organic template provides control over the composition of the product. Initially, the positively charged headgroups of the surfactant interact with the polymerizing silica framework, which has a high charge at short synthesis times. After this initial organization period during which the mesophase is formed, the secondary template (TPA^+) can be incorporated into the walls of the growing mesophase. It is interesting to note that the time of addition has a large effect on the ability to form a material that has physical properties of both mesoporous and microporous phases. Adding the template and surfactant simultaneously at the start of the polymerization process, for example, did not produce the desired mixed-phase material. It appears that a particular degree of silica polymerization is required to form a material containing both mesophase and microphase regions. Control of the silica polymerization rate by optimizing the reagent concentrations, the initial aging time prior to TPA^+ addition, and crystallization time and temperature allowed us to identify a set of conditions under which the meso- and microphases could be simultaneously observed.

Figure 1 shows the powder X-ray diffraction (XRD) patterns between 2θ values of 1−7° and 7−30° for Ti-MMM-2 samples that were crystallized for varying time intervals between 12 and 80 h. The initial stirring time at room temperature (180 min) was the same for all samples. The XRD pattern after 12 h is typical of the MCM-48 mesophase belonging to the $Ia\bar{3}d$ space group,[1−3] with the (211) and (220) diffraction peaks appearing at 2θ values of 2.6 and 3.0°, respectively. The diffraction peaks between $2\theta = 3.5$ and 6.0° are also characteristic of the $Ia\bar{3}d$ space group, and the fact that these peaks are broad and low-intensity indicates that the regions of ordering within the sample are somewhat small. The region between $2\theta = 7$ and 30° contains a broad peak centered at approximately $2\theta = 25°$. This feature has been attributed to noncrystalline silica within the walls of the mesophase.[32] Figures 1b and c show XRD patterns for Ti-MMM-2 samples which have been crystallized for time intervals of 20 and 30 h, respectively. As seen from these figures, an increase in the crystallization time beyond 12 h resulted in formation of mixed-phase material, as seen by the presence of diffraction peaks corresponding to the $Ia\bar{3}d$ mesophase at low angles and diffraction peaks between 7 and 30° corresponding to a crystalline microporous phase. The peaks in the higher 2θ region show a gradual increase in intensity as crystallization time increases. At prolonged heating times, the intensities of these peaks match well with the XRD pattern of a pure TS-1 sample. This is also consistent with the use of TPA^+ as the secondary template, since TPA^+ has been shown to play a role in the formation of the MFI zeolite structure type on which TS-1 is based.[33] The appearance of the TS-1 phase coincides with an increase in broadening of the Ti-MCM-48 peaks and a decrease in peak intensities for samples crystallized for more than 20 h. Indeed, the Ti-MMM-2 sample crystallized for 50 h (Figure 1d) shows a broad, low-intensity peak in the mesophase region that cannot be indexed to the $Ia\bar{3}d$ structure. These changes are attributed to the formation of TS-1 within the pore system of Ti-MCM-48 in a nonuniform manner throughout the entire material, thereby leading to smaller regions of ordering in the mesophase as the crystallization of the zeolite progressed. Crystallization of the reaction mixture beyond 50 h led to the formation of sample containing only a single broad peak at $2\theta = 2.0°$ in addition to the microporous phase; in contrast to the other samples, the mesoporous peak disappeared after calcination (Figure 1e). This indicates the presence of a highly disordered, unstructured mesophase that collapses upon calcination. Thus, XRD studies clearly show the transformation of the mesophase to microphase as a function of crystallization time.

IR spectroscopy, also an important tool used for characterizing zeolitic phases, is frequently used to differentiate between the atomic-level ordering in crystalline zeolites and the amorphous nature of mesoporous materials. A strong, prominent band at approximately 550 cm^{-1} in zeolites is characteristic of five-ring T−O−T structures in microporous silicates,[20,22] where T = Si, Al, or Ti. This band is absent in mesoporous materials, which lack atomic-level ordering. Figure 2 shows the IR spectra of TS-1, Ti-MCM-48, and various Ti-MMM-2 samples in the region of 400−1600 cm^{-1}. The IR spectrum of Ti-MCM-48 shows bands at 1230, 1084, 810, and 460 cm^{-1}, due to symmetric/asymmetric stretching vibrations and bending vibrations of Si−O−Si bonds. The band at approximately 970 cm^{-1} is attributed to stretching vibrations of Si−O−R functionalities, where R = H or a metal ion. The IR spectrum of a Ti-MMM-2 sample crystallized for 12 h matches closely with that of Ti-MCM-48, indicating a close resemblance between the two samples and the presence of primarily mesophase in this sample, consistent with the above XRD studies. On the other hand,

TABLE 1: Summary of Physical Data for Ti-MCM-48, Ti-MMM-2, and TS-1 Samples

sample[a]	phase	average pore diameter (Å)	pore volume (cm^3/g)	surface area (m^2/g)	$Q_{4Crys}/(Q_4+Q_3+Q_2)_{Amorph}$
Ti-MCM-48	meso	30.6	1.01	1319	0
Ti-MMM-2-12	meso	32.6	1.25	1369	0.21
Ti-MMM-2-20	meso+micro	32.2	1.12	1364	0.33
Ti-MMM-2-30	meso+micro	30.5	0.92	1360	0.47
Ti-MMM-2-50	meso+micro	28.8	0.64	967	0.70
Ti-MMM-2-80	micro	[b]	0.17	399	2.19
TS-1	micro	[b]	0.10	351	∞

[a] For Ti-MMM-2 samples, the last number (12, 20, etc.) indicates the crystallization time at 150 °C. [b] Average pore diameter was smaller than accurately measurable by instrument.

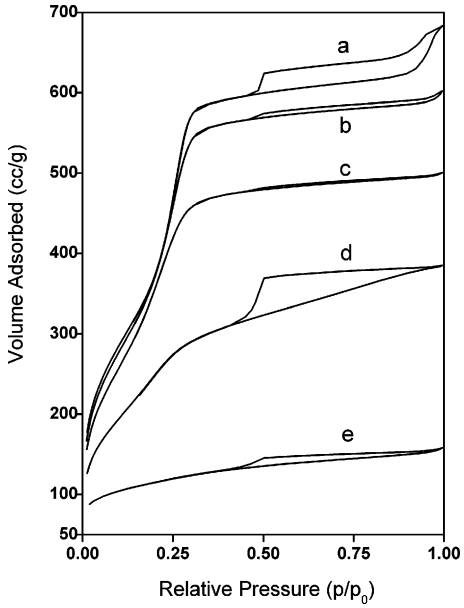

Figure 3. Nitrogen physisorption isotherms of calcined Ti-MMM-2 samples crystallized at 150 °C for (a) 12 h, (b) 20 h, (c) 30 h, (d) 50 h, and (e) 80 h.

Ti-MMM-2 samples crystallized for 20, 50, and 80 h show, in addition to the various vibrational bands present in the 12 h sample, a new and prominent band at 550 cm^{-1}, which is found to grow progressively as a function of aging time. This band indicates development of the microporous phase in these samples (again consistent with XRD). Also observed in these samples are bands present at about 590 and 630 cm^{-1}. The presence of such bands is generally attributed to nanophase silicalite material,[34] indicating formation of nanocrystalline TS-1 particles in products. The IR spectrum of a Ti-MMM-2 sample crystallized for 80 h (Figure 2e) matches closely with that of pure TS-1, indicating that the sample contains almost exclusively the crystalline, microporous phase.

Nitrogen physisorption isotherms for the Ti-MMM-2 samples are shown in Figure 3. The adsorption−desorption isotherm for Ti-MMM-2 crystallized for 12 h is a typical type IV isotherm, with a sharp inflection point at partial pressures of 0.2−0.4 due to capillary condensation. This inflection is characteristic of mesoporous materials.[35] However, the isotherm of Ti-MMM-2 samples which were crystallized for longer times show a decrease in the total adsorbed volume of nitrogen; in addition, the inflection point decreases in sharpness and shifts to lower partial pressure values. These changes result in a gradual conversion of the isotherm from type IV to type I (characteristic of microporous materials) as crystallization time increases. These results are consistent with the above XRD and IR studies, which show formation of the TS-1 phase in these samples along with a simultaneous decrease in the mesoporous character as a function of crystallization time. On the basis of these data and data from other research, we can conclude that the changes in the isotherms indicate that the TS-1 is distributed throughout the pores of the mesoporous phase material in an inhomogeneous manner.[36] An additional feature of the physisorption isotherms is the presence of hysteresis between the adsorption and desorption branches of the isotherms, which can be observed due to capillary condensation effects particularly at relative pressures (p/p_0) greater than 0.4. However, this feature has also been attributed to the presence of interconnected pores of different sizes,[37] which is consistent with a material containing both micro- and mesopores, although the size of the hysteresis does not follow a particular trend. MCM-48 samples prepared with gemini surfactants also show this feature even in the absence of a microporous template, which may indicate the hysteresis is due to the textual modulation of the pore surface in addition to the interconnected micro- and mesopores.

The surface areas, average pore diameters, and pore volumes of Ti-MMM-2 samples are given in Table 1. Ti-MMM-2 crystallized for 12 and 20 h showed a larger surface area and pore volume than Ti-MCM-48. These samples also show a slightly larger average pore diameter than Ti-MCM-48. Importantly, the fact that the pore size, surface area, and pore volume all increase simultaneously indicates that the pores are not significantly blocked during the initial stages of microphase formation. At longer crystallization times (more than 30 h), the pore diameter, surface area, and pore volume all decrease as more of the microporous phase is formed. This is consistent with a progressive increase in the peak widths of the pore size distribution plots (Figure 4). This behavior is indicative of inhomogeneous formation of TS-1 within an increasingly disordered Ti-containing mesophase, thus leading to an overall decrease in the measured diameters of the mesoporous phase. Similarly, the decreases in the surface area and pore volume are assigned to formation of a microporous phase that has a lower surface area and pore volume than the mesoporous phase.

Solid-state ^{29}Si MAS NMR spectra of various Ti-MMM-2 samples after calcination are presented in Figure 5. The spectrum of Ti-MMM-2 crystallized for 12 h shows a broad peak at −107 ppm with a shoulder at less negative field. This type of peak indicates a mixture of several different types of tetrahedrally coordinated Si atoms: (1) Q^4, those connected to four other Si atoms through oxygen atoms, chemical shift ∼−110 ppm; (2) Q^3(OR), those connected to three other Si atoms and one heteroatom through oxygen atoms, chemical shift ∼−95 to −105 ppm; (3) Q^3, those connected to only three other Si atoms through oxygen atoms, with the fourth coordination site occupied by −OH or $-O^-$, chemical shift ∼−100 ppm; and (4) Q^2, those connected to only two other Si atoms through oxygen atoms, with the fourth coordination site occupied by −OH or $-O^-$, chemical shift ∼−90 ppm. The broadness of the Ti-MMM-2 peak in Figure 5a is characteristic of amorphous silica and is

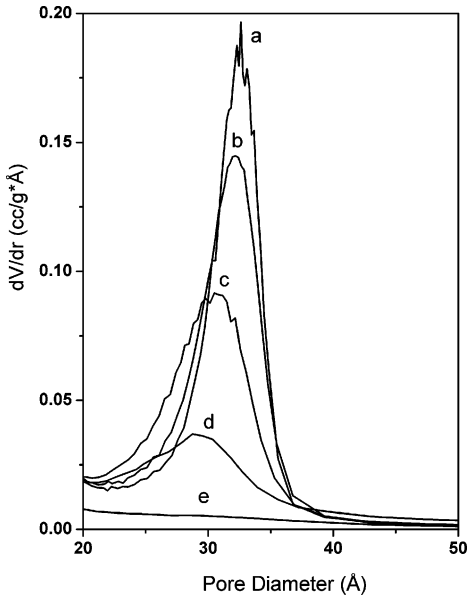

Figure 4. Pore size distribution plots of calcined Ti-MMM-2 samples crystallized at 150 °C for (a) 12 h, (b) 20 h, (c) 30 h, (d) 50 h, and (e) 80 h. The BJH equation was used to calculate the distributions.

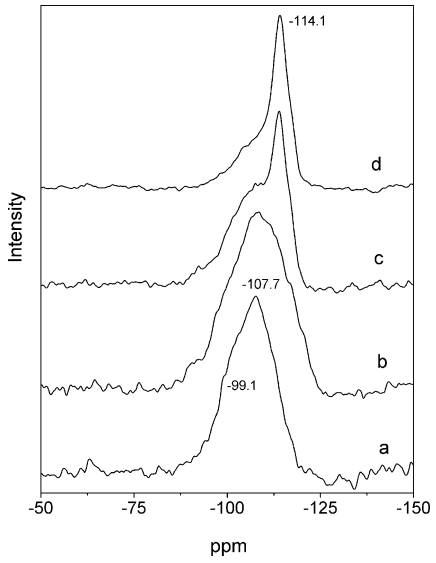

Figure 5. ^{29}Si MAS NMR spectra of calcined Ti-MMM-2 samples crystallized at 150 °C for (a) 12 h, (b) 20 h, (c) 50 h, and (d) 80 h.

frequently observed for mesoporous materials. The chemical shift of −107 ppm indicates that a majority of the Si atoms are in Q^4 environments following calcination; the shoulder at a less negative chemical shift is more difficult to deconvolute due to the overlapping chemical shifts of Q^3(OR) and Q^3 Si atoms. However, we can conclude that the majority of the Si atoms are in fully polymerized (Q^4 or Q^3(OR)) environments, with a smaller number of Si atoms in Q^3 and Q^2 environments. This result is consistent with the fact that siliceous MCM-48 (no Ti) shows a ratio of Q^4/Q^3 greater than 1, with somewhat sharper peaks.[30,38]

As the crystallization time is increased to 20 h, the NMR peak first becomes broader as a shoulder with a more negative chemical shift appears. At even longer crystallization times, a peak appears at −114 ppm that is significantly more narrow than the broad peak due to amorphous silica. This new peak is characteristic of the Q^4 sites in microporous silicates such as ZSM-5 and TS-1, in which the Si−O−Si bonds are crystallographically oriented so that significantly more of the Si atoms

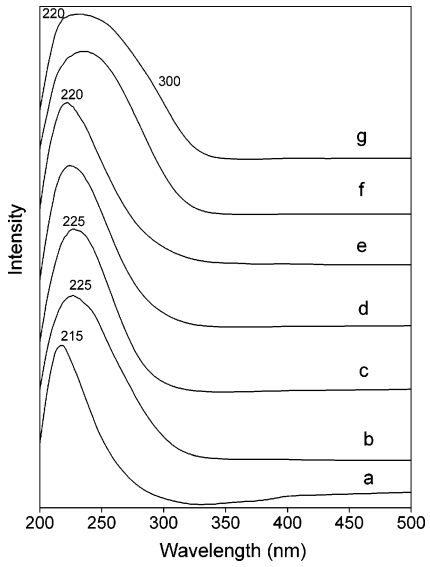

Figure 6. DR UV/Vis spectra of (a) TS-1, (b) Ti-MCM-48, and calcined Ti-MMM-2 samples crystallized at 150 °C for (c) 12 h, (d) 20 h, (e) 30 h, (f) 50 h, and (g) 80 h.

are in the same chemical environments.[39] This was confirmed by obtaining the NMR spectrum of TS-1 alone, which showed a single peak at −114 ppm. The NMR spectra of the Ti-MMM-2 samples could be deconvoluted following the growth of the crystalline Q^4 peak, to quantify the relative amounts of Si atoms in crystalline and amorphous environments and therefore determine the relative amounts of microporous and mesoporous phases in the samples. The ratio of peak areas defined as $Q^4_{cryst}/(Q^4 + Q^3 + Q^2)_{amorph}$ increased from an initial ratio of 0.33 in the Ti-MMM-2 sample crystallized for 20 h to a value of 2.19 in the sample crystallized for 80 h (Table 1). This relative growth of the crystalline peak with the concomitant decrease in the amorphous peak is consistent with the overall transformation of Ti-MCM-48 mesophase to the TS-1 microphase.

Diffuse reflectance UV−visible spectroscopy (DR-UV/Vis) is a very common method used to study the coordination environment of Ti in porous silicates. Figure 6 shows the DR-UV/Vis spectra of TS-1, Ti-MCM-48, and Ti-MMM-2 samples. All of the samples, except for Ti-MMM-2 crystallized for 50 and 80 h, show an absorption peak between 210 and 240 nm. It is well-known that the bands in these regions for Ti-silicates arise due to charge transfer from oxygen to tetrahedral Ti in the crystalline framework sites of zeolites.[40] The spectrum of pure TS-1 shows a relatively sharp and narrow absorption band at 215 nm, consistent with previous reports that indicated the presence of Ti in a tetrahedral coordination environment.[40] In contrast, the spectrum of Ti-MCM-48 shows an absorption band centered at about 225 nm that is comparatively broader than the peak in the TS-1 spectrum. The slight red shift and increase in the width of this band is generally attributed to a distorted tetrahedral Ti environment, believed to be due to amorphous character of the pore walls (i.e., the wide range of Ti−O−Si bond angles) in mesoporous material.[41] The DR-UV/Vis spectrum of Ti-MMM-2 crystallized for 12 h closely matches that of Ti-MCM-48, indicating a close structural similarity between these samples, which is consistent with the other experimental data. Spectra of samples crystallized for 20 and 30 h showed peaks that were shifted to lower wavelengths, with increasing peak widths. These changes are indicative of the presence of both microporous and mesoporous phases within the sample. The absence of peaks between 230 and 260 nm, which have been reported to indicate the presence of octahedrally coordi-

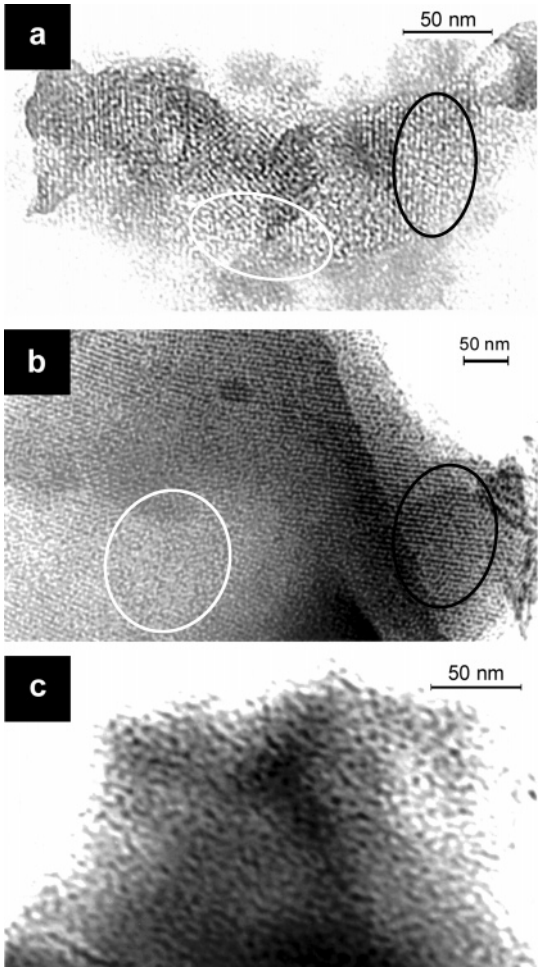

Figure 7. TEM images of Ti-MMM-2 samples crystallized at 150 °C for (a) 20 h, (b) 30 h, and (c) 50 h. Black ellipses indicate regions of mesopore ordering; white ellipses indicate regions of disorder.

nated Ti, indicate that Ti-MMM-2 samples contain the catalytically active four-coordinate Ti species. The trends in peak position and width continues as the crystallization time increased to 50 and 80 h. The peaks in the spectra for these samples are unusually broad, which is due to development of a new band at approximately 300 nm in addition to the peak at lower wavelengths. This new band could be due to breakdown of the mesophase, leading to Ti−O−Ti clustering in which the Ti atoms are present in an octahedral environment. The existence of this type of peak has been reported earlier for Ti−O−Ti bonds in silicon-rich amorphous phases.[14]

Transmission electron microscopy (TEM) was used to study the particle morphologies and the pore ordering in Ti-MMM-2 samples. Figure 7 shows representative TEM images of Ti-MMM-2 samples crystallized for 20, 30, and 50 h. Ti-MMM-2 samples crystallized for 20 and 30 h do show some regions of mesopore ordering, typical of the $Ia\bar{3}d$ phase observed along the (110) and (100) directions.[42] However, many regions of disorder are also observed in these samples. This is consistent with the XRD spectra of these samples, which show prominent (211) and (220) peaks of the $Ia\bar{3}d$ phase, while at the same time the peaks in the region between $2\theta = 3$ and 6° are quite broad and unresolved, indicating short pore ordering lengths within the samples. In contrast, the TEM image of Ti-MMM-2 crystallized for 50 h shows a highly disordered mesophase, with areas where the structure has totally collapsed, resembling a foam. Regions of ordered mesoporous structure were not observed anywhere in this sample, again consistent with XRD data which showed only very broad, low-intensity diffraction peaks for the mesoporous phase. Interestingly, the average particle size of the TS-1 domains as calculated from the Scherrer equation was found to be 20 to 28 nm for samples crystallized for 20 to 80 h; particle size was found to increase as a function of crystallization time. However, no segregated or isolated microporous particles of this size were visible anywhere in the sample by TEM. The XRD and TEM data from our paper are similar to those found by other researchers for mixed-porosity materials.[17,21,22] Given the XRD, N_2 physisorption, and microscopy data for these samples, this result leads to a model in which the larger TS-1 particles observed by XRD are formed through growth of smaller TS-1 nanoparticles within the walls of the mesoporous phase. Careful examination of the TEM images in Figure 7 does show some features that could be attributed to regions of larger microporous ordering. We are currently pursuing higher-resolution TEM experiments on these samples to examine these features.

TABLE 2: Catalysis Data for Epoxidation of Cyclohexene Using TS-1, Ti-MCM-48, and Ti-MMM-2 as Catalysts

sample	conversion (%)	selectivity (%)	turnover number (mol cyclohexene converted/mol Ti)	[b]turnover frequency (h^{-1})
Ti-MCM-48	41.5	97.7	123	5.1
[a]Ti-MMM-2-12	60.0	94.3	177	7.4
Ti-MMM-2-20	60.4	97.7	178	7.4
Ti-MMM-2-30	61.4	97.2	181	7.5
Ti-MMM-2-40	50.5	95.1	150	6.2
Ti-MMM-2-50	26.6	72.4	78	3.3
TS-1	15.8	18.0	47	1.9

[a] For Ti-MMM-2 samples, the last number (12, 20, etc.) indicates the crystallization time at 150 °C.

TS-1 titanosilicates have been extensively used as catalysts for a number of oxidation and epoxidation reactions, both for fundamental studies as well as for commercial applications.[43,44] However, the small pore sizes of these materials limits their utility for reactions involving larger and bulkier molecules. For these molecules, Ti-doped mesoporous materials have been found to show good activity, although the conversions and selectivity are quite different from TS-1. This is likely due to the lack of atomic ordering in the inorganic walls of these materials. Given the unique physical characteristics of Ti-MMM-2, we were interested in comparing its activity and selectivity to that of TS-1 and Ti-MCM-48 for a given reaction. Oxidation of cyclohexene with *tert*-butyl hydroperoxide (TBHP) was chosen as a test reaction since cyclohexene is relatively large compared to the pore diameter of TS-1 (<7 Å), and this reaction has industrial applications. Catalysis data are presented in Table 2. Cyclohexene oxide was the major product formed during the reaction (56.5 to 59.5%), with minor amounts of 2-cyclohexen-1-ol and 2-cyclohexen-1-one (1.8 to 3.5%) also detected. TS-1 shows lower activity than Ti-MCM-48, which is attributed to its smaller pore size, making it difficult for cyclohexene to interact with the active Ti atoms present within the pores. In comparison, Ti-MMM-2 samples showed higher activity than either TS-1 or Ti-MCM-48. In addition, Ti-MMM-2 samples showed an activity that was unique from a simple physical mixture of TS-1 and Ti-MCM-48, which strongly suggests that the structure of Ti-MMM-2 does not consist of segregated regions of micro- and mesoporosity. Ti-MMM-2 samples that had been crystallized for 20 and 30 h showed the highest activity, suggesting that these materials possesses a unique mixed phase structure which provides an improved reactivity for epoxidation, with the Ti atoms in a local environment that enhances their ability to catalyze this reaction. In addition, the

selectivities of the Ti-MMM-2 crystallized for 20 and 30 h for cyclohexene oxide were comparable to that of Ti-MCM-48 but were remarkably higher than the selectivity of TS-1. Ti-MMM-2 samples that were crystallized for 50 h showed lower activities than that of the Ti-MCM-48 sample. This is consistent with the XRD and N_2 physisorption data, which showed formation of microphase to a greater extent in these samples along with a simultaneous decrease in the mesophase, leading to materials with smaller pore sizes. The activity results thus indicate that mixed phase materials act as superior and efficient catalysts as compared to microporous and mesoporous titanosilicates individually.

Conclusions

Ti-MCM-48/TS-1 (Ti-MMM-2) mixed phase materials were synthesized using a dual template system and following a simple one-pot synthesis method using the gemini surfactant 18-12-18 as the primary (mesophase) organic template and TPA^+ as the secondary (microphase) organic template. The relative amounts of micro- and mesophase in the materials were controlled by changing the crystallization time at 150 °C. Samples crystallized for time intervals between 20 and 50 h showed the presence of both TS-1 and Ti-MCM-48. XRD, N_2 physisorption, and DR-UV/Vis indicated that formation of TS-1 within the mesophase occurred in an inhomogeneous manner. XRD and TEM revealed a gradual disordering in the mesophase as the function of crystallization time, while IR spectroscopy indicated the formation of T−O−T five-membered rings (T = Si or Ti), showing that the crystallization step introduced atomic-level ordering into the materials. The incorporation of Ti species into the silicate framework was supported by DR-UV/Vis studies. The Ti-MMM-2 materials, particularly those crystallized for 20 and 30 h, showed very high conversions for epoxidation of cyclohexene, much better than TS-1 and Ti-MCM-48, with a higher selectivity for cyclohexene oxide.

References and Notes

(1) Beck, J. S.; Vartuli, J. C.; Roth, W. J.; Leonowicz, M. E.; Schmitt, K. D.; Chu, C. T. W.; Olson, D. H.; Sheppard, E. W.; McCullen, S. B.; Higgins, J. B.; Schlenker, J. L. *J. Am. Chem. Soc.* **1992**, *114*, 10834.

(2) Biz, S.; Occelli, M. L. *Catal. Rev.-Sci. Eng.* **1998**, *40*, 329.

(3) Corma, A. *Chem. Rev.* **1997**, *97*, 2373.

(4) Trong On, D.; Desplantier-Giscard, D.; Danumah, C.; Kaliaguine, S. *Appl. Catal. A* **2001**, *222*, 299.

(5) Taguchi, A.; Schüth, F. *Microporous Mesoporous Mater.* **2005**, *77*, 1.

(6) Tanev, P. T.; Chibwe, M.; Pinnavaia, T. J. *Nature* **1994**, *368*, 321.

(7) Corma, A.; Navarro M. T.; Perez-Pariente, J. *J. Chem. Soc., Chem. Commun.* **1994**, 147.

(8) Koyano, K. A.; Tatsumi, T. *Chem. Commun.* **1996**, 145.

(9) Bhaumik, A.; Tatsumi. T. *J. Catal.* **2000**, *189*, 31.

(10) Chen, L. Y.; Chuah, G. K.; Jaenicke, S. *J. Mol. Catal. A: Chem.* **1998**, *132*, 281.

(11) Pena, M. L.; Dellarocca, V.; Rey, F.; Corma, A.; Coluccia, S.; Marchese, L. *Microporous Mesoporous Mater.* **2001**, *44*−*45*, 345.

(12) Tatsumi, T.; Koyano, K. A.; Igarashi, N. *Chem. Commun.* **1998**, 325.

(13) Thomas, J. M. *Angew. Chem., Int. Ed.* **1999**, *38*, 3589.

(14) Notari, B. *Stud. Surf. Sci. Catal.* **1988**, *37*, 413.

(15) Kloetstra, K. R.; van Bekkum, H.; Jansen, J. C. *Chem. Commun.* **1997**, 2281.

(16) Karlsson, A.; Stöcker, M.; Schmidt, R. *Microporous Mesoporous Mater.* **1999**, *27*, 181.

(17) Huang, L.; Guo, W.; Deng, P.; Xue, Z.; Li, Q. *J. Phys. Chem. B* **2000**, *104*, 2817.

(18) Guo, W.; Xiong, C.; Huang, L.; Li, Q. *J. Mater. Chem.* **2001**, *11*, 1886.

(19) Liu, Y.; Zhang, W.; Pinnavaia, T. J. *Angew. Chem., Int. Ed.* **2001**, *40*, 1255.

(20) On, D. T.; Kaliaguine, S. *Angew. Chem., Int. Ed.* **2002**, *41*, 1036.

(21) Prokesova, P.; Mintova, S.; Cejka, J.; Bein, T. *Microporous Mesoporous Mater.* **2003**, *64*, 165.

(22) Xia, Y.; Mokaya, R. *J. Mater. Chem.* **2004**, *14*, 863.

(23) Han, Y.; Xiao, F.-S.; Wu, S.; Sun, Y.; Meng, X.; Li, D.; Lin, S.; Deng, F.; Ai, X. *J. Phys. Chem. B* **2001**, *105*, 7963.

(24) Lin, K.; Sun, Z.; Lin, S.; Jiang, D.; Xiao, F.-S. *Microporous Mesoporous Mater.* **2004**, *72*, 193.

(25) Schmidt, I.; Krogh, A.; Wienberg, K.; Carlsson, A.; Brorson, M.; Jacobsen, C. J. H. *Chem. Commun.* **2000**, 2157.

(26) Poladi, R. H. P. R.; Landry, C. C. *Microporous Mesoporous Mater.* **2002**, *52*, 11.

(27) Poladi, R. H. P. R.; Landry, C. C. *J. Solid State Chem.* **2002**, *167*, 363.

(28) Gallis, K. W.; Landry, C. C. *Chem. Mater.* **1997**, *9*, 2035.

(29) Landry, C. C.; Tolbert, S. H.; Gallis, K. W.; Monnier, A.; Stucky, G. D.; Norby, P.; Hanson, J. C. *Chem. Mater.* **2001**, *13*, 1600.

(30) Huo, Q.; Margolese, D. I.; Stucky, G. D. *Chem. Mater.* **1996**, *8*, 1147.

(31) Morey, M.; Davidson, A.; Stucky, G. D. *Microporous Mater.* **1996**, *6*, 99.

(32) Zhang, W.-H.; Shi, J.-L.; Wang, L.-Z.; Yan, D.-S. *Chem. Mater.* **2000**, *12*, 1408.

(33) Baerlocher, C.; Meier, W. M.; Olson, D. H. *Atlas of Zeolite Structure Types*, 5th ed.; Elsevier: Amsterdam, 2001.

(34) Naik, S. P.; Chiang, A. S. T.; Thompson, R. W.; Huang, F. C. *Chem. Mater.* **2003**, *15*, 787.

(35) Sing, K. S. W.; Everett, D. H.; Haul, R. A. W.; Moscou, L.; Pierotti, R. A.; Rouquerol, J.; Siemieniewska, T. *J. Pure Appl. Chem.* **1985**, *57*, 603.

(36) Luan, Z.; He, H.; Zhou, W.; Cheng, C. F.; Klinowski, J. *J. Chem. Soc., Faraday Trans* **1995**, 2955.

(37) Webb, P. A.; Orr, C. *Analytical Methods in Fine Particle Technology*; Micromeritics Inst. Co.: Norcross, GA, 1997.

(38) Engelhardt, G.; Michel, D. *High-Resolution Solid-State NMR of Silicates and Zeolites*; Wiley: New York, 1987.

(39) Fyfe, C. A.; Gobbi, G. C.; Kennedy, G. J. *J. Phys. Chem.* **1984**, *88*, 3248.

(40) Boccuti, M. R.; Rao, K. M.; Zecchina, A.; Leofanti, G.; Petrini, G. *Stud. Surf. Sci. Catal.* **1989**, *48*, 133.

(41) Zhang, W.; Fröba, M.; Wang, J.; Tanev, P. T.; Wong, J.; Pinnavaia, T. J. *J. Am. Chem. Soc.* **1996**, *118*, 9164.

(42) Sun, J.-H.; Coppens, M.-O. *J. Mater. Chem.* **2002**, *12*, 3016.

(43) Bhaumik, A.; Tatsumi, T. *J. Catal.* **1998**, *176*, 305.

(44) Gallot, J. E.; Kapoor, M. P.; Kaliaguine, S. *AIChE J.* **1998**, *44*, 1438.